IEEE Access
Multidisciplinary ⋮ Rapid Review ⋮ Open Access Journal

Received 10 February 2025, accepted 17 March 2025, date of publication 31 March 2025, date of current version 11 April 2025.

Digital Object Identifier 10.1109/ACCESS.2025.3556334

RESEARCH ARTICLE

Numerical Modeling of PMSM Noise Reduction by Harmonic Current Injection

FEDERICO SORESINI, DARIO BARRI, FEDERICO BALLO, AND MASSIMILIANO GOBBI
Department of Mechanical Engineering, Politecnico di Milano, 20156 Milan, Italy

Corresponding author: Massimiliano Gobbi (massimiliano.gobbi@polimi.it)

This work was supported by the Centro Nazionale per la mobilità sostenibile (MOST)–Sustainable Mobility Center funded by Next-GenerationEU (Piano Nazionale di Ripresa e Resilienza (PNRR)–MISSIONE 4, COMPONENTE 2, INVESTIMENTO 1.4–D.D. 1033), in June 2022, under Grant CN00000023.

ABSTRACT In this paper, harmonic components are injected into the phase current of a Permanent Magnet Synchronous Motor (PMSM) used in automotive applications to improve the Noise Vibration and Harshness (NVH) performance. The study proposes and validates a numerical method for modeling this phenomenon. The strategy was first applied experimentally. Subsequently, the experimental currents were measured and used as input for the numerical models developed in Flux2D (Registered trademark) and Abaqus (Registered trademark). The harmonic contributions of the experimental currents, obtained from the inverter control strategy, are analysed and adopted as inputs to the electromagnetic model to calculate the forces. These are applied to the Finite Element Model (FEM), which returns the values of vibration and acoustic emission of the motor as the injection strategy is varied. The numerical results are then compared and validated with the experimental data. The strategy is applied as an NVH countermeasure to a specific time order that is particularly noisy for the analyzed PMSM. This order turns out to be dominated by a spatial 0 mode also referred to as the breathing mode. The phase of the injected current harmonic is varied between 0 and 2π. For a specific phase angle, a minimum of the acoustic emission level is reached. The application of the strategy experimentally shows a maximum reduction of 29 dB and 27 dB from the vibration and acoustic levels respectively. Numerical models are able to capture the physics of the system, reproducing the variation in acoustic emission as a function of the phase angle of the injected current. Numerical results are close to the experimental data, with a maximum difference of 3dB on the optimal vibration reduction condition.

INDEX TERMS Current injection, PMSM, electric motors, NVH, numerical model, experimental measures, sound emission, countermeasures.

I. INTRODUCTION

Permanent Magnet Synchronous Motors (PMSMs) are a widely adopted motor configuration in the automotive industry, due to their high efficiency, compactness, reliability, high torque, and power density [1]. To ensure these performances, high-efficient speed and current control strategies are required. The controller parameters depend on the characteristics of the PMSM and are managed through various adaptive control strategies, with Artificial Intelligence-based approaches increasingly emerging. [2]. However, these motors exhibit limitations in NVH performance [3]. Many articles in the literature have addressed this topic and different reviews have been published [4], [5], [6], [7]. Due to the progress of electrification in the automotive field, the minimization of vibrations and noise emissions from electric powertrains is a task that needs to be addressed at the design stage. This has led, for the first time, to the inclusion of NVH performance in the formulation of the electric motor multi-objective optimization problem [8], [9], [10], [11]. NVH aspects can no longer be addressed separately from efficiency optimization. Many authors in the literature agree that the major contribution to the noise emitted by an electric motor is derived from the electromagnetic forces that act on the stator teeth [7], [12], [13], [14]. In an electric machine, electromagnetic forces vary both in time and in space. In case of PMSMs, electromagnetic harmonic orders of vibration can be divided into two families, namely orders excited by

The associate editor coordinating the review of this manuscript and approving it for publication was Giovanni Angiulli.

rotating magnetic forces with a spatial lobed shape and orders excited by pulsating forces (i.e. the 0th or breathing mode) [15], [16]. The main vibrational modes of the stator structure are typically excited by low-order rotating forces for two main reasons [11], [17]:

- the natural frequency of low order structural modes may fall inside the frequency range of the rotating machine,
- the modal stiffness of the structure increases with m^4 (being m the spatial order), meaning that low-order structural modes exhibit a higher vibration amplitude for the same input force.

The Great Common Divisor (GCD) between the number of poles $2p$ and slots N_s allows identifying the lowest number of spatial lobes of the electromagnetic force r_{min} [16]. Also, the family of pulsating forces has a relevant contribution in the total noise emission, due to the coupling with 0th mode. The lowest time order affected by this breathing mode corresponds to the least common multiple (lcm) of N_s and $2p$ [16], [18]. In particular, when the spatial deformation and frequency of the electromagnetic force coincide with those of the mechanical system, the structure is excited in a resonance region and a high level of acoustic noise is generated [4]. Several actions can be taken to reduce motor noise emission: slots-poles combination, rotor skewing, modulation control strategies. The slot and pole configuration plays a crucial role in both acoustic and electromagnetic performance, as it determines the excitation frequencies and the vibration modes of the stator. In fact, the radial harmonic force components are primarily influenced by the interaction between the magnets and the armature field. An optimized slot-pole architecture can be employed to reduce noise and vibration in electric motor [16], [19].

Rotor skewing is a commonly employed technique to reduce electromagnetic-induced vibrations, torque ripple and cogging torque in PMSMs [20], which however implies an additional effort in the manufacturing phase. In particular, rotor skewing selectively weakens certain radial force time-harmonic components, shifting them to lower time orders as the skewing angle increases. However, this comes at the cost of torque reduction, requiring a trade-off between noise mitigation and torque loss [21], [22], [23].

Other noise reduction techniques consist in the application of modulation control strategies, that allow to reduce the noise related to the switching frequency of the pulsewidth modulation (PWM) inverter strategy [24]. These methods are effective in reducing the switching losses of the inverter and are able to reduce the noise generated in the high-frequency region, however, such an approach may be less effective in case of high-speed motors, being the frequency range very high and outside the audible region [25].

For this reason, the harmonic current injection technique [26] can be considered as a valid alternative for reducing the noise level and discomfort felt by the vehicle occupants [27]. A proper management and control of such harmonics is a crucial aspect for the effectiveness of the method, since the stator vibration is governed by the space and time harmonic contributions of the electromagnetic forces [4], [14], [15], [17], [28]. Many papers state that the 0^{th} spatial mode, also known as breathing mode, has a major influence on the vibration of traction electric motors [18], [29]. In addition, current injection strategies are more effective on this mode of vibration than on higher spatial orders [9]. An early work on the application of current injection was conducted by Pellerey et al. [30], who studied the effect of the presence of additional current harmonics to the fundamental one by means of numerical simulations. The authors compared simulations with purely sinusoidal currents against the case with the introduction of higher harmonics. An increase of 17 dB was found when considering the case with the addition of higher current harmonics. Numerical simulations were experimentally validated in a second study [31], in which the presence of harmonics in the motor input currents led to an increase in noise emissions of 18 dB in the specific operating conditions. Similarly, Geoffriault et al. [32] introduced a compensation strategy capable of decreasing vibrations by acting on current harmonics. Harries et al. [18] studied the noise reduction for a 30 slots 20 poles Interior Permanent Magnet Synchronous Machines (IPMSM), for hybrid vehicle application, via harmonic current injection. In the paper, a control algorithm to reduce air gap field harmonics was developed by means the application of optimised harmonic stator currents. Numerical results showed a reduction of more than 30 dB μm/s of the mean surface velocity. Harries et al. in [33] and [34] also studied the injection of flux-linkage harmonics to optimise the sound emission of a PMSM for automotive applications. They limited the current injection optimisation problem to two degrees of freedom, namely the amplitude and temporal phase position of the harmonic flux, focusing on reducing mode zero vibrations. Through experimental bench tests, they obtained a reduction in the sound pressure level of the car of approximately 10 dB compared to a field-oriented control, no FEM models were used. Xu et al. [35] proposed a method to suppress the 0th mode vibration of PMSMs, they combined shape optimisation of permanent magnets and harmonic current injection. The latter can change the phase difference of the concentrated force harmonics on the tooth, transforming zero mode vibration into non-zero mode vibration. Considering another approach aimed at maximizing the benefit of vibration reduction for the 0th-order mode, Wang et al. [36] propose a novel PMSM current injection strategy where the injected current harmonic is selected based on the estimation of the zero-order natural frequency of the stator. Also Langheck et al. [11] performed NVH optimization by modifying the current trajectory in the $d-q$ plane with the harmonic current injection strategy. Experimental results show that the harmonic generated in the current counteracts the force that excites the acoustic noise, decreasing the emission by about 30 dB at the resonance peak. Ciceo et al. [14] introduced a novel current shaping method for a 3-phase PMSMs that has demonstrated significant reductions in torque ripple and radial air-gap force harmonics

under MTPA conditions, resulting in improved NVH performance across the speed range. Windisch et al. [37], in their work, focused mainly on defining current injection strategies, useful for determining current orders, amplitudes and phases to reduce noise emission. They presented an open-loop harmonic injection strategy to reduce tonal noise in IPMSM, the method includes a pre-calculation of noise-cancelling feed-forward voltage amplitudes and phases. While Jiang and Wang in [25] proposed an analytical harmonic current design method for tangential noise suppression of vehicular electric drives. The proposed method relies on FEA model's accuracy. Bassani et al. [26] developed an active vibration control technique based on current injection with the aim of reducing a single torque harmonic. Experimentally, they vary amplitude and phase of the injected current resulting in a maximum reduction in acceleration levels of 29 dB at a specific frequency. Finally, Fu et al. [9] propose a guideline for developing an harmonic current injection control method for NVH optimization of a PMSM model, taking into account the influence of structural characteristics.

As highlighted in the literature review, most studies on harmonic current injection focus primarily on control logic and, at best, present experimental findings based on the application of different injection strategies. Other studies attempt to model numerically the phenomenon providing only partial representations, lacking a validated comprehensive modeling approach that traces the process from current injection to the motor's acoustic emission. This paper aims to bridge this gap by presenting a general modeling method capable of capturing the reduction in vibration and noise emissions of PMSMs induced by the application of a current injection strategy. The proposed approach includes both the analysis of electromagnetic forces and the resulting vibrations through mechanical modeling, capturing the physics of the system. It allows for the validation of different current injection strategies with results that correlate with experimental evidence. The approach leverages experimentally measured current waveforms coupled with electromagnetic and vibro-acoustic models of the electric machine. The measured input current is fed as input to the electromagnetic model of the PMSM to compute the radial and tangential components of the induced forces acting on the stator structure. The computed forces are mapped on the tooth head of a structural model of the stator by means of the nodal transfer method [4] to compute the external surface vibration and the related noise radiation. The proposed framework serves as a tool for investigating noise reduction strategies through harmonic injection on a numerical basis, enabling the development and testing of various methods for noise mitigation. In particular, for the analysed motor, a specific target is the noise emission associated with mode 0, which has been identified as the main contributor in the analyzed frequency range.

In section II, current harmonics injection theory is presented explaining the relationship between the time orders of currents versus those of electromagnetic forces and vibrations. In section III the case study is presented, the main characteristics of the motor are shown as well as the experimental measurements carried out. Next, Section IV presents the numerical modelling process employed to estimate the noise emission reduction from experimental currents with the presence of injected harmonics. The section includes the evaluation of electromagnetic forces, the description of the structural FEM model and of the acoustic volume. Finally, in section V the numerical results are analysed and compared with the experimental tests. A final discussion of the results obtained is also reported.

II. CURRENT HARMONICS AND ELECTROMAGNETIC FORCES IN A PMSM

Permanent Magnet Synchronous Motors are rotating field machines, in which the control strategy is performed in the d-q rotor fixed system. In a standard system, the currents i_d and i_q, which control the operation of the electric motor, are typically constant and non-oscillating [38]. The implemented current injection strategy introduces a higher-order harmonic into the i_d and i_q currents supplied by the inverter.

Current injection intends to reduce the vibration excited by specific time orders of the electromagnetic force. Therefore, selecting the appropriate order for the additional current injected into the dq system is essential [31], [39]. The relationship between currents, fluxes and forces orders is schematically summarised in Fig. 1.

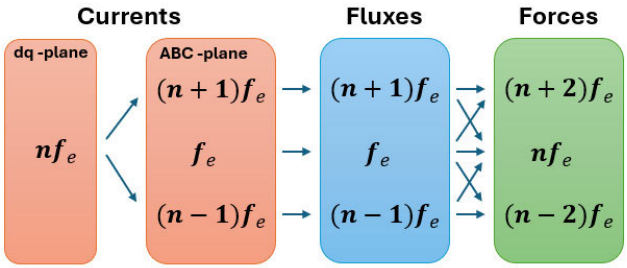

FIGURE 1. Relationship between currents, fluxes and forces orders.

A. DQ – ABC CURRENT TRANSFORMATION

The current contributions of i_d and i_q can be defined as

$$i_d = i_{d0} + A_{i_d} \cos(n\omega t + \phi_d) \quad (1)$$

$$i_q = i_{q0} + A_{i_q} \cos(n\omega t + \phi_q) \quad (2)$$

where i_{d0} and i_{q0} are respectively the constant values of current i_d and i_q employed to guarantee the operating performance required, A_{i_d} and A_{i_q} are the amplitude of the injection harmonic currents, while ϕ_d and ϕ_q are the related phases. $\omega = 2\pi f_e$ is the circular frequency of the fundamental current. Once the reference i_d and i_q are defined, current amplitudes in the three-phase system (abc coordinates) can

be obtained by the inverse Park transform [40]

$$\begin{bmatrix} a \\ b \\ c \end{bmatrix} = \begin{bmatrix} \cos(\omega t) & -\sin(\omega t)) & 1 \\ \cos(\omega t) - \frac{2\pi}{3}) & -\sin(\omega t) - \frac{2\pi}{3}) & 1 \\ \cos(\omega t) + \frac{2\pi}{3}) & -\sin(\omega t) + \frac{2\pi}{3}) & 1 \end{bmatrix} \begin{bmatrix} d \\ q \\ 0 \end{bmatrix} \quad (3)$$

In practice, to reduce the acoustic emission on an order nf_e (with f_e the fundamental frequency), it is necessary to introduce a damping force of the same order. This is obtained from currents in the dq plane with order nf_e. Moving to the plane ABC (three-phase plane), in addition to the fundamental current f_e, currents orders $(n+1)f_e$ and $(n-1)f_e$ are obtained. These orders are also reflected in the contribution of flux harmonics [28], [41], [42].

B. FORCE HARMONICS

The air gap field in PMSM is composed of permanent-magnet field and armature reaction field, where the stator slotting effect can be considered by a relative permeance function. Considering only the radial component of the flux density, it can be expressed as [41]

$$b_r = [B_{r_{mag}}(\theta, t) + B_{r_{arm}}(\theta, t)]\lambda(\theta) \quad (4)$$

where t is the time, θ is the stator angle, $B_{r_{mag}}(\theta, t)$ and $B_{r_{arm}}(\theta, t)$ are the slotless radial permanent magnet field and slotless radial armature reaction field, respectively. $\lambda(\theta, t)$ is the relative permeance function. $B_{r_{mag}}(\theta, t)$, $B_{r_{arm}}(\theta, t)$ and $\lambda(\theta)$ can be expressed by Fourier series as [28]

$$B_{r_{mag}}(\theta, t) = \sum_{\alpha} B_{m\alpha} \cos(\alpha p\theta - \alpha 2\pi f_e t) \quad (5)$$

$$B_{r_{arm}}(\theta, t) = \sum_{k} \sum_{v} B^k_{av} \sin(vN_t\theta - s_{v,k} 2\pi k f_e t + \theta_k) \quad (6)$$

$$\lambda_r(\theta) = \lambda_0 + \sum_{\mu} \lambda_{r\mu} \cos(\mu N_s \theta) \quad (7)$$

where p is the number of pole pairs, N_s is the number of slots, N_t is the number of spatial period of the motor, f_e is the fundamental current frequency, k is the order of current harmonics and θ_k is the related phase angle. B^k_{av} is the amplitude of vN_t-th harmonic of armature reaction given by current harmonics at a frequency kf_e, finally $s_{v,k}$ indicates the sign of the armature reaction field rotation.

The radial force density reads

$$p_r(\theta, t) = \frac{[B_{r_{mag}}(\theta, t) + B_{r_{arm}}(\theta, t)]^2 \lambda_r^2(\theta)}{2\mu_0} \quad (8)$$

Substituting eqs. 5, 6, 7 into eq. 8 and keeping only the lowest spatial order of the electromagnetic force [28] we get

$$\begin{aligned} p_r \approx\ & \frac{1}{4\mu_0}\lambda_0 \sum_{\alpha_1}\sum_{\alpha_2}\sum_{\mu=1}^{\infty} \lambda_{r\mu} B_{m\alpha_1} B_{m\alpha_2} \\ & \times \{\cos\{[(\alpha_1+\alpha_2)p \pm \mu N_s]\theta - (\alpha_1+\alpha_2)2\pi f_e t\} \\ & + \cos\{[(\alpha_1-\alpha_2)p \pm \mu N_s]\theta - (\alpha_1-\alpha_2)2\pi f_e t\}\} \\ & + \frac{1}{2\mu_0}\lambda_0^2 \sum_{\alpha}\sum_{k}\sum_{v} B_{m\alpha} B^k_{av} \\ & \times \big\{\sin\{[(\alpha p + vN_t) \pm \mu N_s]\theta - (\alpha + s_{v,k}k)2\pi f_e t + \theta_k\} \\ & - \sin\{[(\alpha p - vN_t) \pm \mu N_s]\theta - (\alpha - s_{v,k}k)2\pi f_e t - \theta_k\}\big\} \\ & + \frac{1}{2\mu_0}\lambda_0 \sum_{\alpha}\sum_{k}\sum_{v}\sum_{\mu=1}^{\infty} \lambda_{r\mu} B_{m\alpha} B^k_{av} \\ & \times \big\{\sin\{[(\alpha p + vN_t) \pm \mu N_s]\theta - (\alpha + s_{v,k}k)2\pi f_e t + \theta_k\} \\ & - \sin\{[(\alpha p - vN_t) \pm \mu N_s\}\theta - (\alpha - s_{v,k}k)2\pi f_e t - \theta_k\}\big\} \end{aligned} \quad (9)$$

where the armature reaction field contribution is present in the second and third term of eq. 9. The presence of k^{th} harmonic in the current yields harmonics $(\alpha \pm s_{v,k}k)f_e$ (where α is and odd number) in the radial force. Considering only the fundamental field of the permanent magnet, which has the largest amplitude ($\alpha = 1$) and neglecting the sign, the force frequencies result equal to $(1 \pm k)f_e$ [28], [41], [42]. Now considering the k^{th} current harmonic as $k = n \pm 1$, we obtained that in addition to the order of the desired force nf_e, two other harmonic components at orders $(n+2)f_e$ and $(n-2)f_e$ are generated (see Figure 1).

C. TORQUE RIPPLE

Torque ripple represents a critical aspect in PMSMs as it can generates unwanted vibrations, it includes: cogging torque, permanent magnet torque ripple and reluctance torque ripple. The former depends on the combination of stator slots and rotor poles, while the latter are originated by harmonic components of the flux and harmonic components of the stator current. [43]. The force harmonics generated in the airgap, particularly their tangential component, affect the motor's torque ripple [44]. For this reason, current injection techniques are adopted also as a modern control method to reduce torque ripple [14], [45], [46]. This reduction not only extends the life of the drivetrain and improves comfort but also plays a significant role in lowering the overall noise emissions of the electric motor.

III. EXPERIMENTAL TESTS

The motor under analysis is a PMSM for automotive applications featuring 12 poles and 18 slots, a typical architecture of electric motor for automotive traction [47], [48]. It features a concentrated winding stator and a surface permanent magnet rotor. The reference motor parameters are reported in Table 1.

TABLE 1. Reference motor parameters.

Parameter	Value	Unit
Stator outer diameter	140	mm
Stator bore	80	mm
Gap	2.5	mm
Stack length	100	mm
Number of Turns	26	
Max power	100	kW
Max current	500	A

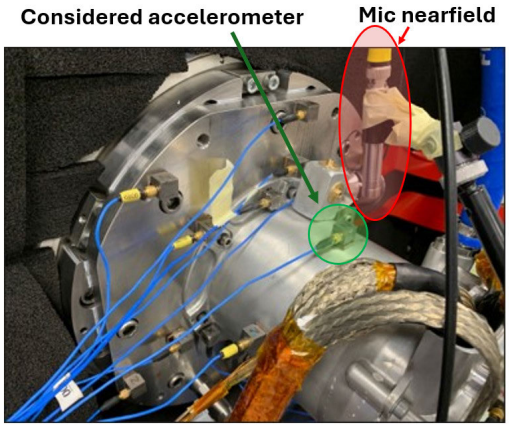

FIGURE 2. Experimental set-up.

In the test bench, two identical motors are mounted in a back-to-back configuration, with one of the two acting as a generator/brake. The tractive motor is equipped with a PCB 339A30 tri-axial accelerometer with a nominal sensitivity 10 mV/g, positioned on the outer surface of the housing. A near-field acoustic measurement is carried out, where a PCB HT378B02 microphone with a nominal sensitivity of 50 mV/Pa is positioned 50 millimeters from the motor surface, in front of the accelerometer. The experimental set-up is shown in Fig. 2.

The input currents fed by the inverter were measured with three alternating current probes, placed directly on an unsheathed part of the electrical cable to avoid disturbances caused by eddy currents. Data acquisition and processing is performed via LMS Testlab [49]. The absolute position of the rotor was deducted by the current waveforms in post-processing stage.

The objective is to reduce vibration and acoustic emission associated with the 6th harmonic of the electrical frequency ($6f_e$). For this motor architecture, this specific harmonic order is characterized by an amplitude and a frequency range (up to 2500 Hz) that is particularly annoying to the human ear. For this reason, a current injection mitigation technique has been adopted and applied at the same order $6f_e$ to reduce vibrations, as explained in section II-A. This method, as supported by the literatures [9], [18], and [29] is particularly effective when applied to harmonics characterized by a 0^{th} spatial force component, as is the case here.

A speed ramp from 0 to 4000 rpm at the maximum continuous torque T_{max} was set and measurements were taken both without current injection (baseline condition) and with injection strategy enabled. When the injection strategy was enabled, a total of 36 tests were executed, for each test a different value of phase angle ϕ_q of the q-current was imposed, while keeping the same amplitude A_{i_q}, which was set to 30 A corresponding to the 6% of the rated current. This choice ensures a negligible decrease in system efficiency. The phase angle ϕ_q is varied over a range from 0° to 360°. In this first study, it was decided to inject only i_q current, similarly to other works in literature [26]. This choice was also supported by preliminary experimental activities, which showed the introduction of i_d to have a minor influence on NVH performance than i_q current. This can be easily explained by the fact that the i_q current governs the delivered torque, so it is the main cause of the forces acting on the system [11]. Moreover, the predominant use of current i_q over the i_d in harmonic current injection is supported by the literature [39].

A. CURRENTS

In this study, a $6f_e$ time order harmonic in the i_d-i_q plane has to be introduced. This results in the two side harmonics $5fe$ and $7fe$ (i.e. the $(n \pm 1) f_e$) in the a, b, c domain (see Figure 1) [31], [32]. The motor input currents are controlled by the inverter logic. The three-phase output currents of the inverter have been measured by means of AC current clamps, in this way, the effective current waveforms generated by the inverter can be employed to compute the noise emission, thus avoiding the need of a numerical model of the inverter machine, which is out of the scope of the paper. It is worth emphasizing that modeling the actual control logic of the inverter is a complex task that requires specific models. Anyway, the control logic of the inverter could be included in the loop by means of a digital twin of the inverter. The harmonic content of the measured current waveforms has been extracted by an angle domain order tracking [50]. In addition to fundamental current harmonic f_e, which remains quite constant over the frequency range, also the $5f_e$ and $7f_e$ harmonics present a relevant contribution. These orders are already present in the analysis of the baseline case without injection strategy. The presence of higher current harmonics depends on the control technique, asymmetric impedance, back-EMF harmonics and dead time of the inverter [32], [51], [52]. In Fig. 3 and 4 the experimental current amplitude of harmonics $5fe$ and $7fe$ are shown as function of rpm and injected ϕ_q (i_q phase angle) for an A_{i_q} equal to 30 A. As can be seen from the graphs, the amplitude currents of the two orders show, for a constant phase angle, a decreasing trend with the speed. Ideally, being the motor working in the range of constant torque (and current), this trend should be constant and independent on the rotational

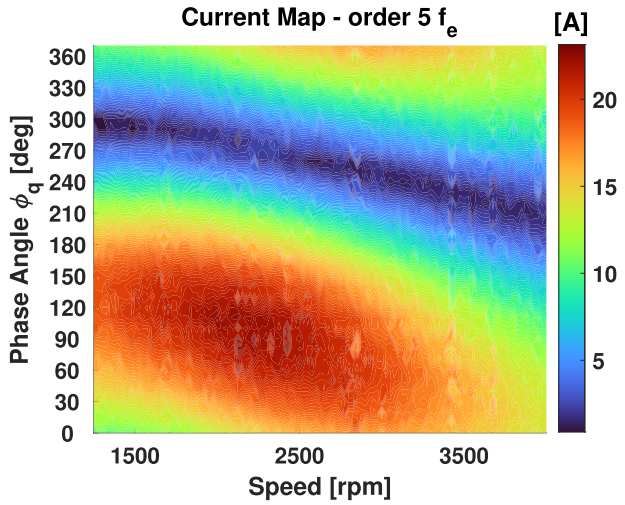

FIGURE 3. Experimental current map order 5 f_e.

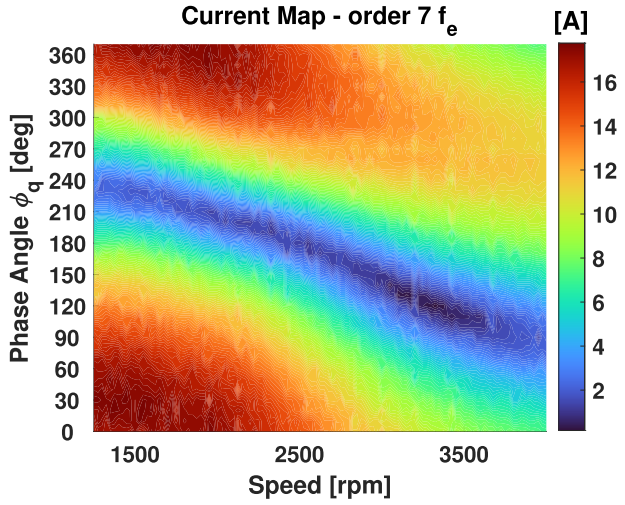

FIGURE 4. Experimental current map order 7 f_e.

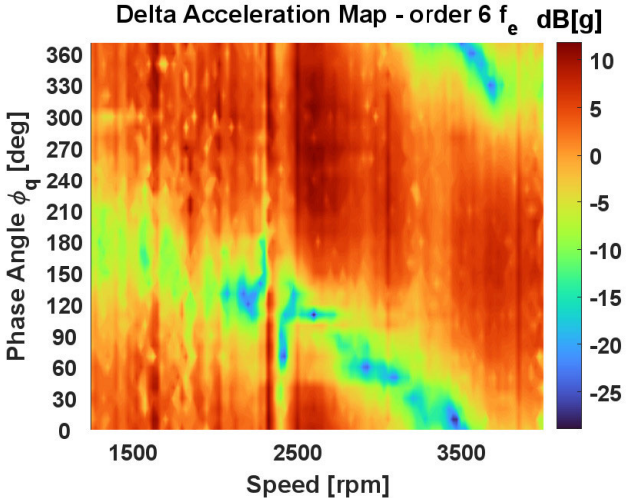

FIGURE 5. Vibrations reduction map for an injected current A_{i_q}=30A.

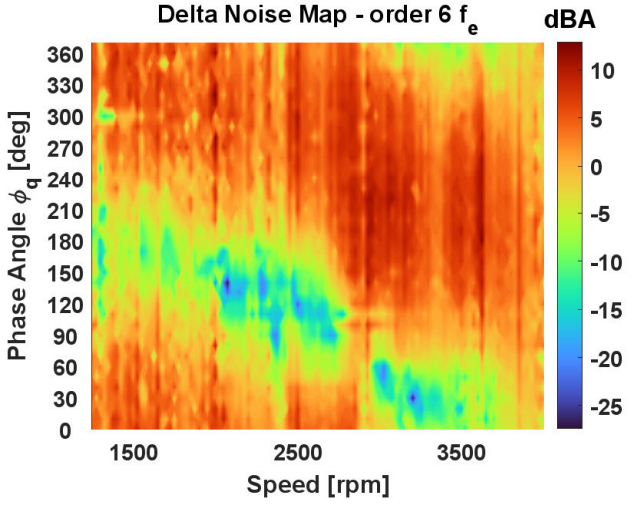

FIGURE 6. Noise reduction map for an injected current A_{i_q}=30A.

speed of the motor. This could be a consequence of the (non-ideal) control logic of the inverter, which introduces spurious harmonics to maintain the constant current reference while increasing the motor speed.

B. VIBRATION AND NOISE

In Fig. 5 and 6 the maps of vibration and noise level variations with respect to the baseline case are shown respectively. In particular, Figure 5 shows the variation of the radial acceleration measured by the accelerometer with respect to the baseline condition (dB scale) as function of the motor speed and phase angle ϕ_q. A similar plot is reported in Figure 6, where the sound pressure level variation with respect to the baseline condition (dBA scale) is shown in place of the radial acceleration. Both figures show a distinct blue band where the vibration and the acoustic emission are lowered by several dB. In particular, a maximum reduction of 29 dB and 27 dBA is achieved for vibration and noise emission, respectively. These results are consistent with other studies reported in the literature [26].

IV. NUMERICAL MODEL

In this section, the general method for modelling the effect of current injection on NVH performances of the PMSM is presented. The modelling approach and the experimental validation procedure are schematised in Figure 7. The measured three-phase current waveforms provided by the inverter, which include the side harmonics introduced by the current injection strategy, are fed to an electromagnetic model of the PMSM developed in Flux2D®. By this model, the electromagnetic forces acting on the tooth heads are computed. These forces are then input into a Finite Element Model (FEM) of the electric motor created in Abaqus®, where steady-stated dynamic structural simulations at various rotational speeds are conducted to compute motor vibrations. Finally, through the modelling of an air volume, the acoustic

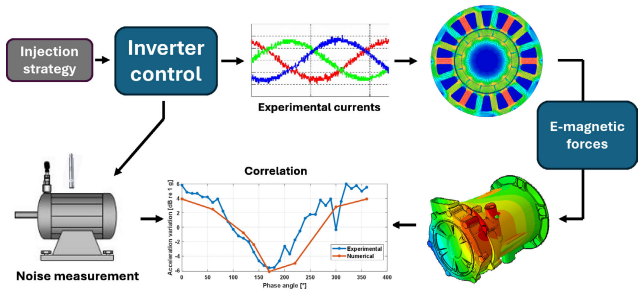

FIGURE 7. Process.

emission of the PMSM is evaluated. Numerical results are then compared with the experimental data to validate the method.

A. INPUT CURRENTS

In the electromagnetic simulation software Flux2D®, the experimental currents are reconstructed in order to reproduce the experimental operating points. The input currents are defined as the sum of the three harmonics of order f_e, $5f_e$ and $7f_e$ respectively, considering the correct initial phase shift of the model. The formulation of the three phase currents are

$$I_a(t) = \sum_{k\in\{6,30,42\}} I_{ak}\cos(\frac{k}{2p}\omega t + \phi_{ak}) \tag{10}$$

$$I_b(t) = \sum_{k\in\{6,30,42\}} I_{bk}\cos(\frac{k}{2p}\omega t + \phi_{bk}) \tag{11}$$

$$I_c(t) = -(I_a(t) + I_b(t)) \tag{12}$$

Since harmonic magnitudes vary across rpm and phase angles ϕ_q, simulations were performed for selected speeds: 1500 rpm and 2500 rpm.

B. ELECTROMAGNETIC FORCES

The calculation of the electromagnetic forces is carried out in Flux2D® with a linear mesh model with 21 nodes on the tooth head. This number has been obtained from a sensitivity analysis in which the number of nodes was increased until convergence was reached on the value of the resultant force on the tooth. For a defined operating speed, the electromagnetic load case is defined by the temporal and spatial distribution. The forces were then decomposed using the Fast Fourier transform (FFT) to analyse each operating condition. A two-dimensional representation of the time and space order of the electromagnetic force of the motor is reported in Fig. 8. The three main force contributions are characterised by spatial orders 6 and 0. The spatial order 6 (r_{min}) has the largest contribution on time order $2f_e$ and a minor one on $4f_e$, while the spatial mode zero has the main contribution on time harmonic $6f_e$. As can be seen from the graph, the contribution (0, 6) is greater for tangential forces than for radial forces. In addition, for tangential forces, contribution (0, 6) is second in order of amplitude just after the contribution (6, 2). Although the zero space mode, at the force level is not the main contribution, at the noise emission

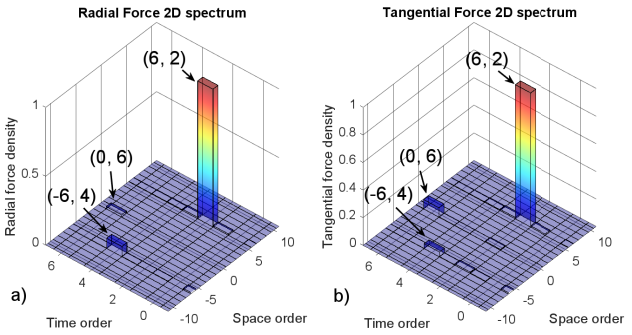

FIGURE 8. 2D force spectrum: a) Radial force, b) Tangential force.

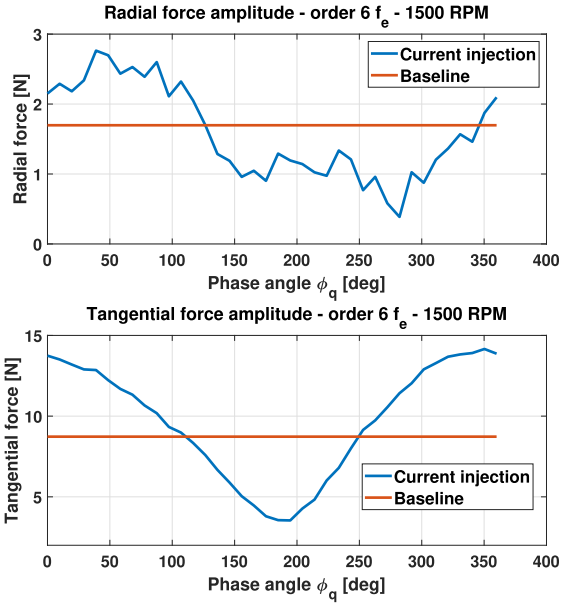

FIGURE 9. Radial and tangential forces variation - 1500 rpm.

level it gives rise to one of the main NVH problems of electric motors. For this reason, the analysis focuses on temporal order $6f_e$, which appears to be critical for the noise emitted by the motor considered. The resultant radial and tangential forces was then calculated for a selected tooth. The results obtained are shown in Fig. 9, 10, for speeds of 1500 and 2500 rpm respectively. The graphs show that the variation of the radial and tangential force amplitude follows a clear trend as a function of the injected current phase angle ϕ_q. In general, tangential forces exhibit greater peak-to-peak variation as a function of injected phase than radial forces. They also show a smoother behaviour with respect to the radial one. The minimum force point, as a function of the injected phase ϕ_q, varies for both radial and tangential components and for the two considered rotational speeds.

C. TORQUE RIPPLE

The main component of torque ripple of the considered motor acts on the $6f_e$ temporal order. This means that the current injection strategy will also affect the torque ripple variation. An electromagnetic simulation has been performed at a

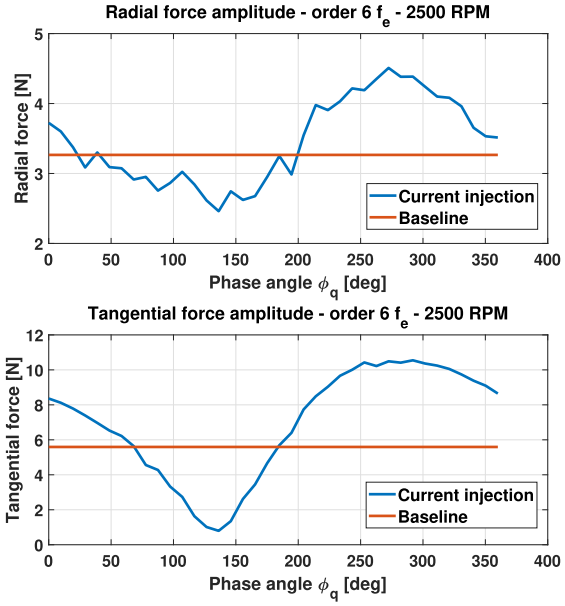

FIGURE 10. Radial and tangential forces variation - 2500 rpm.

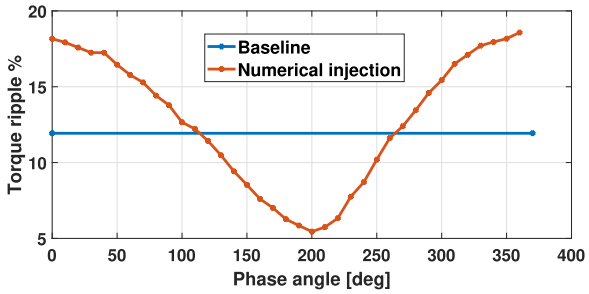

FIGURE 11. Torque ripple.

TABLE 2. Stator core materials physical properties.

	Description	Steel	Varnishing	Resin	Copper	Units
E	Young's modulus	185	1	10	115	GPa
G	Shear modulus	71.1	0.37	3.7	43.2	GPa
ν	Poisson's ratio	0.3	0.35	0.35	0.33	
ρ	Density	7650	2350	2350	8960	kg/m^3
v	Volume fraction	0.96	0.04			

TABLE 3. Equivalent computed stator core transversely isotropic properties.

	Description	Value	Units
$E_X = E_Y$	Young's modulus: X,Y direction	175.8	GPa
E_Z	Young's modulus: Z direction	18.1	GPa
ν_{XY}	Poisson coefficient: XY plane	0.3	
$\nu_{XZ} = \nu_{ZY}$	Poisson coefficient: XZ, ZY plane	0.3022	
G_{XY}	Shear modulus: XY plane	67.62	GPa
$G_{XZ} = G_{ZY}$	Shear modulus: XZ, ZY plane	59.57	GPa

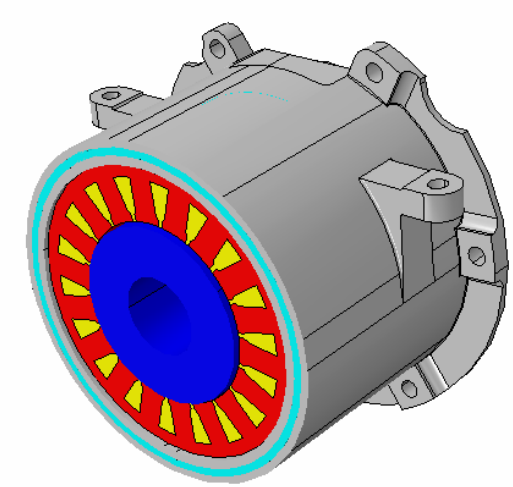

FIGURE 12. Finite element model representation of the PMSM.

rotational speed of 1500 rpm. Figure 11 shows the amount of torque ripple expressed as a percentage of the provided torque compared to the baseline case (i.e. with no current injection). From the figure it emerges that selecting an i_q phase angle equal to 200° allows to halve the amount of torque ripple with respect to the baseline case. This confirms that the proposed method can be effectively applied also for reducing torque fluctuations in PMSMs [45], [46]. Interestingly, the phase angle that minimizes the torque ripple coincides with the one that minimizes the tangential forces (see Figure 9).

D. STRUCTURAL MODEL

The numerical structural model of the PMSM has been realised by a FEM approach in Abaqus® software. The electric motor was modeled in its main parts, namely stator lamination, winding, slot insulation, jacket, rotor and cooling fluid. The modelling method is based on the use of the physical parameters of the materials (Table 2), without relying on a model based on identified parameters obtained by correlations with experimental tests. To account for lamination and insulating varnish, the laminated stator was modeled as an homogeneous part made of transversely isotropic material [53]. The equivalent engineering constants of the homogenized material are computed by means of the rule of mixtures, the complete formulation is explained in [54] and [55]. The computed material properties are reported in Table 3, where Z axis corresponds to the motor axis.

The polymeric insulation is represented as a single linear elastic solid that occupies the stator slots. It is rigidly bonded to the stator lamination at the interface surfaces. The elastic modulus of the polymer is scaled according to the effective slot fill, equal to 0.4. The copper windings are modelled as one-dimensional beam elements with equivalent cross section area and moment of inertia computed from the Litz wire. The beam elements are embedded in the polymer insulation material. In order to take into account for dynamic viscous effect a structural damping equal to 0.03 has been assigned to the stator [56]. Figure 12 depicts the complete structural model of the PMSM. The stator case is connected to a grounded plate by kinematic ties located at the connection screws. While the rotor is connected to the jacket via two

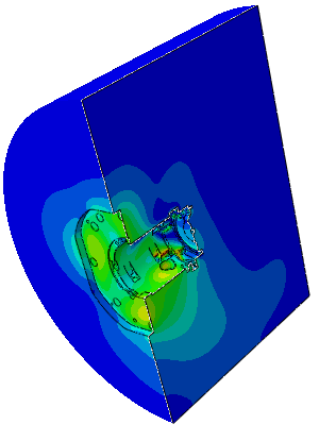

FIGURE 13. Acoustic domain.

bearings modelled by radial springs with equivalent stiffness of $3 \cdot 10^8$ N/m, which has been estimated by the bearings manufacturer [57].

In addition, the cooling fluid was modelled as an acoustic domain in order to consider the fluid-structure interaction in the vibration of the external surface of the stator case [55]. A 50% water/glycol solution has been assumed, with bulk modulus of 3 GPa and a mass density of 1000 kg/m^3. A "tie" constraint has been assigned at the interface surface between fluid and and stator case.

A steady-state dynamic simulation has been performed by considering the physical degrees of freedom of the structure in place of the modal superposition approach. For further details on the modelling procedure, the readers are addressed to [55].

E. ACOUSTIC MODEL

The acoustic model is realised using FEM in Abaqus®. A cylindrical volume of air around the electric motor (Figure 13) was meshed with ACRD4 linear acoustic tetrahedral elements [58], with global mesh size of 4 mm. The element size and dimension of the air volume were defined in accordance with the conditions imposed by the frequency range analysed [55], [58]. The nodal displacements of the motor's outer surface computed by the structural simulation are used as input for the acoustic domain. The sound propagation in the volume of air is simulated by considering the non-reflecting condition at the boundaries of the domain. A submodelling technique is applied to handle air-structure interaction and reduce the computational cost. The sound pressure level (SPL) is extracted from the acoustic simulation for a microphone positioned in the nearfield, at a distance of 50 mm from the motor. The microphone is also visible in the experimental setup image, Fig. 2.

V. RESULTS AND DISCUSSION

Vibration and acoustic tests are conducted to validate the previously described structural and acoustic models. In particular, the microphone measurement is intended to

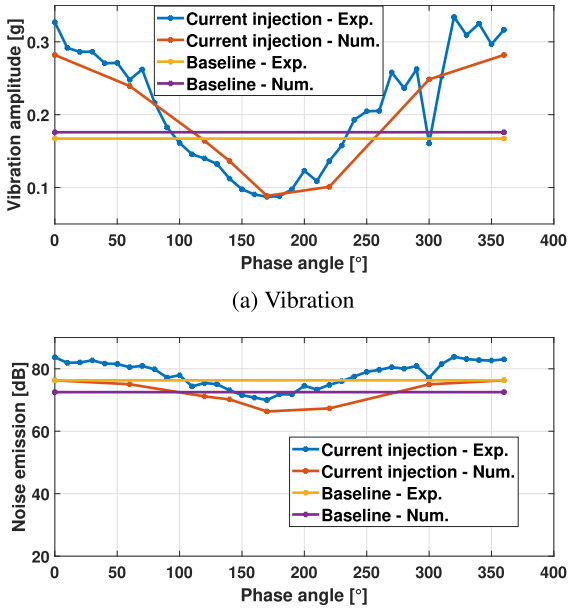

(a) Vibration

(b) Acoustic emission

FIGURE 14. Comparison between numerical results and experimental measures at 1500 rpm.

correlate numerical data and not to provide an acoustic characterization of the motor. In figures 14a and 14b, the numerical results and experimental values about radial vibration and acoustic emission of the motor at 1500 rpm are reported. In the graphs, both baseline and current injection condition at varying injection phase angle are shown. The good level of accuracy of the numerical model can be appreciated from the reduced difference between the numerical and experimental baseline curves, about 5% for both vibration amplitude and noise emission. Similar numerical-experimental correlation level is maintained once the injection strategy is applied. This highlights the strong correlation between numerical results and the experimental measurements, emphasizing the high accuracy of the model in predicting both vibration amplitude and noise emission.

The effect of current injection phase angle on the amplitude of the radial acceleration and acoustic sound pressure level can be more clearly appreciated from graphs 15a and 15b where the curves express the relative variation (in a dB scale) of the acceleration and sound pressure level with respect to the baseline case. In the figures, the measured quantities (blue lines) are compared against the results of the numerical simulation (orange lines). Figures 16a and 16b show the same results but at a different rotational speed of the motor, namely 2500 rpm.

For the 1500 rpm case (Figure 15a and Figure 15b), the maximum reduction of vibration level is obtained for a phase angle around 170°, an analogous trend can be seen for the sound pressure level. Such a behavior is well captured by numerical simulations (orange lines in Figure 15a and Figure 15b), which exhibit a consistent global trend with respect to experimental evidence. A difference of less than

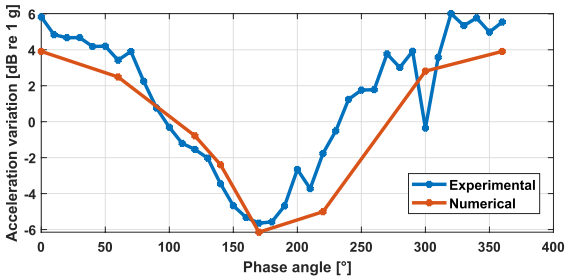

(a) Vibration reduction

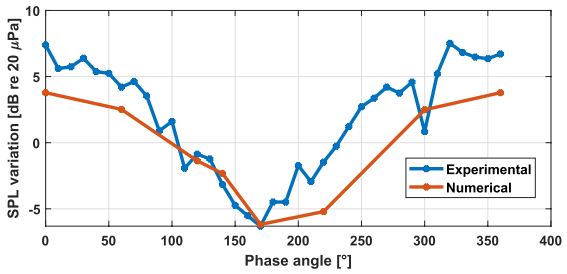

(b) Acoustic emission reduction

FIGURE 15. Comparison between numerical results and experimental measures at 1500 rpm.

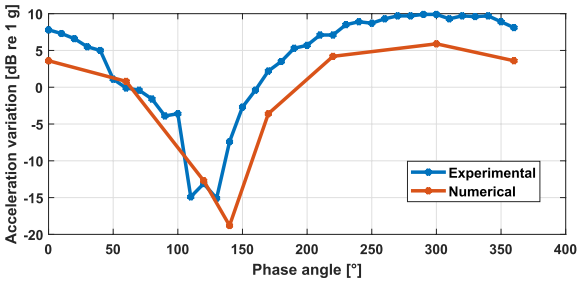

(a) Vibration reduction

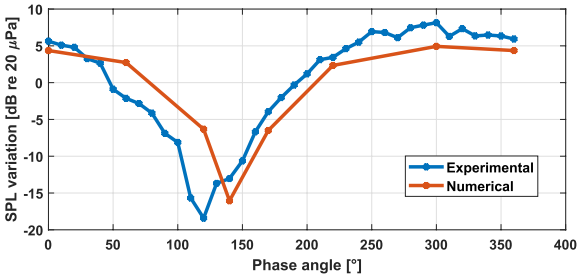

(b) Acoustic emission reduction

FIGURE 16. Comparison between numerical results and experimental measures at 2500 rpm.

1 dB was observed between the numerical and experimental results at the phase angle of maximum vibration reduction, both in terms of acoustic performance and acceleration.

For the 2500 rpm case, a clear minimum is found on the reduction of the vibration and noise levels (Figure 16a and Figure 16b respectively), in this case the the minimum vibration levels are found for a lower phase angle than the 1500 rpm case, namely around 120°. Additionally, it can be observed that with the increase of the rotational speed of the motor the optimal range of phase angles is significantly narrowed, as confirmed by the literature [26]. Even for this condition, numerical simulations (orange lines) exhibit a coherent behavior, with a difference of approximately 3 dB in the maximum vibration reduction. This discrepancy is consistent with findings in other literature sources [59], [60], [61]. In contrast to the 1500 rpm case, the optimum phase angle from the simulations is slightly shifted forward to 140°. The results show that properly selecting the injected phase angle for different rotational speeds allows for an optimal noise reduction. In particular, decreases of 6 dB and nearly 20 dB are achieved at 1500 rpm and 2500 rpm, respectively.

Similarly noise attenuation outputs were obtained in [21], where a rotor skewing mitigation technique was adopted. Increasing the skewing angle led to a greater acoustic reduction, reaching a maximum decrease of approximately 10 dB at specific frequencies for an angle of 4.5°, with a significant torque reduction.

By comparing the curves of Figure 15 and Figure 16, with those of Figure 9 and Figure 10, it can be observed that the optimal phase angle (i.e. the phase angle that minimizes the vibration levels at the two speeds) is the same one that minimizes the amplitude of tangential forces

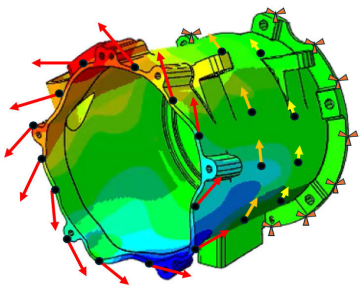

FIGURE 17. Electric motor housing torsional mode.

(see Figure 9 and Figure 10). This suggests that in the analyzed frequency range tangential forces have a greater contribution than radial ones. Such a conclusion is also confirmed by the computed deformation mode shape of motor case shown in Figure 17, which exhibits prevalently a torsional deformation mode.

The experimental validation confirms that the numerical framework proposed in this paper allows for an accurate modeling of the effect of harmonic current injection for minimum noise emission on a PMSM. From a practical point of view, three-phase current maps like those of Figure 3 and Figure 4 are required inputs for the numerical simulations. These quantities may be derived from available experimental data on similar machines or, ideally, by integrating the model of the control inverter in the loop. In any case, the proposed approach allows for an efficient preliminary setting of the inverter control logic. In other words, the proposed method allows for defining amplitude, phase angle and harmonic order of reference input current to be fed to the electric machine to reduce the radiated noise. The obtained setting

represents a starting configuration, which can be further improved and adapted to the specific electric machine by a subsequent fine-tuning of the inverter parameter directly on the test bench.

VI. CONCLUSION

In the paper, the topic of NVH performance maximization of a PMSM via harmonic current injection has been addressed. A comprehensive numerical simulation framework, based on the integration of electro-magnetic and vibro-acoustic models of the electric machine has been proposed. The experimentally validated method enables the estimation of noise reduction in electric motors induced by harmonic current injection strategies. Experimentally-derived current maps of the three-phase input current harmonic components to be injected were provided as input to the electro-magnetic model of the PMSM. These currents were used to compute the related radial and tangential components of the electromagnetic force that excites the structural vibration. The resulting input forces were supplied as input to a vibro-acoustic model of the machine to compute the radiated sound pressure. The method has been applied for the NVH optimization of a 12-poles 18-slots PMSM for automotive applications. Specifically, the aim was to reduce the $6f_e$ time order vibration harmonic, which has the major contribution in the overall radiated sound pressure level for this particular machine architecture. Different values of phase angle of the injected current have been simulated at two different rotational speeds and compared to experimental acquisitions. Results have shown that the numerical simulations allow to compute the optimal phase angle that minimizes the vibration of the electric machine with a maximum error of 15%. In terms of NVH improvement, the proposed method achieved a noise level attenuation of almost 20 dB compared to the case without current injection strategy, considering the harmonic current injected with the optimal phase. Interestingly, for this specific case study, the optimal phase angle also minimizes torque ripple. The proposed method can be generally applied to any radial flux PMSM architecture, enabling the designer to define an optimized harmonic current injection strategy for the power inverter to minimize the noise emission of the electric machine. The implementation of a digital twin of the inverter in the simulation framework allows the method to be totally predictive and independent from experimental measurements. Considering the amplitudes and phases of the input currents as design variables and the reduction in noise emission as the objective function, the entire approach can be viewed as an optimization process. By identifying the most perceptible or annoying harmonics for drivers or users, the process enables the efficient leveraging of injected currents and the determination of optimal injection strategies. Overall, this approach enhances motor performance, by improving driver comfort and compliance with noise regulations across applications such as electric vehicles.

ACKNOWLEDGMENT

This manuscript reflects only the authors' views and opinions.

REFERENCES

[1] S. Lakshmikanth, "Noise and vibration reduction in PMSM—A review," *Int. J. Electr. Comput. Eng.*, vol. 2, no. 3, p. 405, Apr. 2012, doi: 10.11591/ijece.v2i3.322.

[2] A. Fatemimoghadam, L. Varaha Iyer, and N. C. Kar, "Real-time validation of enhanced permanent magnet synchronous motor drive using dense-neural-network-based control," *IEEE Access*, vol. 12, pp. 73323–73339, 2024.

[3] R. M. Pindoriya, B. S. Rajpurohit, and R. Kumar, "A novel application of harmonics spread spectrum technique for acoustic noise and vibration reduction of PMSM drive," *IEEE Access*, vol. 8, pp. 103273–103284, 2020, doi: 10.1109/ACCESS.2020.2999336.

[4] F. Soresini, D. Barri, F. Ballo, M. Gobbi, and G. Mastinu, "Noise and vibration modeling of permanent magnet synchronous motors: A review," *IEEE Trans. Transport. Electrific.*, vol. 10, no. 4, pp. 8728–8745, Dec. 2024, doi: 10.1109/TTE.2024.3365151.

[5] Y. Qin, X. Tang, T. Jia, Z. Duan, J. Zhang, Y. Li, and L. Zheng, "Noise and vibration suppression in hybrid electric vehicles: State of the art and challenges," *Renew. Sustain. Energy Rev.*, vol. 124, May 2020, Art. no. 109782.

[6] P. Song, W. Li, S. Mukundan, and N. C. Kar, "An overview of noise-vibration-harshness analysis for induction machines and permanent magnet synchronous machines," in *Proc. 10th Int. Electr. Drives Prod. Conf. (EDPC)*, Dec. 2020, pp. 1–8.

[7] W. Deng and S. Zuo, "Electromagnetic vibration and noise of the permanent-magnet synchronous motors for electric vehicles: An overview," *IEEE Trans. Transport. Electrific.*, vol. 5, no. 1, pp. 59–70, Mar. 2019.

[8] A. Parpinel, P. Bouvet, and J.-B. Dupont, "NVH multiobjective and robust optimization of electric motor design, including power losses," in *Proc. Inter-Noise Noise-Con Congr. Conf.* Wakefield, MA, USA: Institute of Noise Control Engineering, Oct. 2024, vol. 270, no. 4, pp. 7073–7083.

[9] T. Fu, Z. Xu, M. Günther, S. Pischinger, and S. Böld, "Harmonic injection method for NVH optimization of permanent magnet synchronous motors considering the structural characteristics of the machine," SAE Tech. Papers 2024-01-3015, Jul. 2024, doi: 10.4271/2024-01-3015.

[10] D. Barri, F. Soresini, M. Gobbi, A. D. Gerlando, and G. Mastinu, "Optimal design of traction electric motors by a new adaptive Pareto algorithm," *IEEE Trans. Veh. Technol.*, early access, Jan. 23, 2025, doi: 10.1109/TVT.2025.3532752.

[11] A. Langheck, D. Krahe, P. Breining, D. Stretz, T. Rittgerott, J. Kolb, and M. Doppelbauer, "NVH optimization in PMSM through harmonic current injection with optimum current trajectory," in *Proc. Electromech. Drive Syst., ETG Symp.* Frankfurt, Germany: VDE, Nov. 2021, pp. 1–8.

[12] N. Remus, M. S. Toulabi, S. Mukundan, H. Dhulipati, W. Li, C. Novak, and N. C. Kar, "Electromagnetic noise and vibration in PMSM and their sources: An overview," in *Proc. IEEE Can. Conf. Electr. Comput. Eng. (CCECE)*, Aug. 2020, pp. 1–4.

[13] S. Wu, W. Li, W. Tong, and R. Tang, "Electromagnetic vibration and noise comparison of amorphous metal PMSMs and silicon steel PMSMs," *IEEE Access*, vol. 7, pp. 62672–62680, 2019, doi: 10.1109/ACCESS.2019.2916391.

[14] S. Ciceo, F. Chauvicourt, J. Gyselinck, and C. Martis, "PMSM current shaping for minimum Joule losses while reducing torque ripple and vibrations," *IEEE Access*, vol. 9, pp. 114705–114714, 2021.

[15] F. Soresini, D. Barri, S. Manzoni, F. Ballo, and M. Gobbi, "Modal characterization of a PMSM using different experimental techniques," in *Proc. Int. Conf. Noise Vib. Eng.*, 2024, pp. 2852–2865.

[16] M. Mendizabal, A. McCloskey, J. Poza, S. Zarate, J. Iriondo, and L. Irazu, "Optimum slot and pole design for vibration reduction in permanent magnet synchronous motors," *Appl. Sci.*, vol. 11, no. 11, p. 4849, May 2021, doi: 10.3390/app11114849. [Online]. Available: https://www.mdpi.com/2076-3417/11/11/4849

[17] F. Ballo, M. Gobbi, G. Mastinu, and R. Palazzetti, "Noise and vibration of permanent magnet synchronous electric motors: A simplified analytical model," *IEEE Trans. Transport. Electrific.*, vol. 9, no. 2, pp. 2486–2496, Jun. 2023, doi: 10.1109/TTE.2022.3209917.

[18] M. Harries, M. Hensgens, and R. W. De Doncker, "Noise reduction via harmonic current injection for concentrated-winding permanent magnet synchronous machines," in *Proc. 21st Int. Conf. Electr. Mach. Syst. (ICEMS)*, Oct. 2018, pp. 1157–1162.

[19] Y. Wang, H. Gao, H. Wang, and W. Ma, "NVH optimization analysis of permanent magnet synchronous motor by rotor slotting," *Vehicles*, vol. 2, no. 2, pp. 287–302, May 2020, doi: 10.3390/vehicles2020016. [Online]. Available: https://www.mdpi.com/2624-8921/2/2/16

[20] S. Wang and H. Li, "Effects of rotor skewing on the vibration of permanent magnet synchronous motors with elastic-plastic stator," *IEEE Trans. Energy Convers.*, vol. 37, no. 1, pp. 87–96, Mar. 2022.

[21] X. Wang, X. Sun, and P. Gao, "Study on the effects of rotor-step skewing on the vibration and noise of a PMSM for electric vehicles," *IET Electr. Power Appl.*, vol. 14, no. 1, pp. 131–138, Jan. 2020, doi: 10.1049/iet-epa.2019.0238. [Online]. Available: https://ietresearch.onlinelibrary.wiley.com/doi/abs/10.1049/iet-epa.2019.0238

[22] X. Li, L. Zhang, H. Ying, S. Huang, and Q. Zhang, "Study of suppression of vibration and noise of PMSM for electric vehicles," *IET Electric Power Appl.*, vol. 14, no. 7, pp. 1274–1282, Jul. 2020, doi: 10.1049/iet-epa.2019.0805. [Online]. Available: https://ietresearch.onlinelibrary.wiley.com/doi/abs/10.1049/iet-epa.2019.0805

[23] R. Islam, I. Husain, A. Fardoun, and K. McLaughlin, "Permanent-magnet synchronous motor magnet designs with skewing for torque ripple and cogging torque reduction," *IEEE Trans. Ind. Appl.*, vol. 45, no. 1, pp. 152–160, Mar. 2009, doi: 10.1109/TIA.2008.2009653.

[24] Y. Huang, Y. Xu, W. Zhang, and J. Zou, "Hybrid RPWM technique based on modified SVPWM to reduce the PWM acoustic noise," *IEEE Trans. Power Electron.*, vol. 34, no. 6, pp. 5667–5674, Jun. 2019.

[25] S. Jiang, Y. Wang, and Z. Hu, "Tangential force noise reduction of vehicular PMSM based on reference harmonic current analytical computation," *IEEE Trans. Transport. Electrific.*, vol. 9, no. 2, pp. 2081–2089, Jun. 2023, doi: 10.1109/TTE.2022.3206344.

[26] M. Bassani, D. Pinardi, A. Toscani, E. Manconi, and C. Concari, "Active vibration control via current injection in electric motors," *Electronics*, vol. 13, no. 17, p. 3442, Aug. 2024.

[27] X. Wang, A.-L. Osvalder, and P. Höstmad, "Influence of sound and vibration on perceived overall ride comfort—A comparison between an electric vehicle and a combustion engine vehicle," *SAE Int. J. Vehicle Dyn., Stability, NVH*, vol. 7, no. 2, pp. 153–171, Feb. 2023.

[28] F. Lin, S. Zuo, W. Deng, and S. Wu, "Modeling and analysis of electromagnetic force, vibration, and noise in permanent-magnet synchronous motor considering current harmonics," *IEEE Trans. Ind. Electron.*, vol. 63, no. 12, pp. 7455–7466, Dec. 2016.

[29] A. Hofmann, F. Qi, T. Lange, and R. W. De Doncker, "The breathing mode-shape 0: Is it the main acoustic issue in the PMSMs of today's electric vehicles?" in *Proc. 17th Int. Conf. Electr. Mach. Syst. (ICEMS)*, Oct. 2014, pp. 3067–3073, doi: 10.1109/ICEMS.2014.7014021.

[30] P. Pellerey, V. Lanfranchi, and G. Friedrich, "Coupled numerical simulation between electromagnetic and structural models. Influence of the supply harmonics for synchronous machine vibrations," *IEEE Trans. Magn.*, vol. 48, no. 2, pp. 983–986, Feb. 2012, doi: 10.1109/TMAG.2011.2175714.

[31] P. Pellerey, G. Favennec, V. Lanfranchi, and G. Friedrich, "Active reduction of electrical machines magnetic noise by the control of low frequency current harmonics," in *Proc. 38th Annu. Conf. IEEE Ind. Electron. Soc.*, Oct. 2012, pp. 1654–1659, doi: 10.1109/IECON.2012.6388727.

[32] M. Geoffriault, E. Godoy, D. Beauvois, and G. Favennec, "Active reduction of vibrations in synchronous motors by use of an estimator," in *Proc. IEEE Int. Conf. Control Appl. (CCA)*, Aug. 2013, pp. 808–813.

[33] M. Harries and R. W. De Doncker, "Flux injection with reduced degree of freedom for low vibrations and improved NVH in permanent magnet synchronous machines," in *Proc. 23rd Int. Conf. Electr. Mach. Syst. (ICEMS)*, Nov. 2020, pp. 80–85, doi: 10.23919/ICEMS50442.2020.9291133.

[34] M. Harries, A. Woerndle, and R. W. De Doncker, "Low vibrations and improved NVH in permanent magnet synchronous machines due to injection of flux-linkage harmonics," *IEEE J. Emerg. Sel. Topics Power Electron.*, vol. 10, no. 2, pp. 1649–1657, Apr. 2022, doi: 10.1109/JESTPE.2021.3092711.

[35] Z. Xu, G. Yu, Y. Xu, and J. Zou, "Zeroth-mode vibration suppression through adjustment on phases difference of concentrated force harmonics for PMSMs," *IEEE Trans. Magn.*, vol. 58, no. 8, pp. 1–6, Aug. 2022, doi: 10.1109/TMAG.2022.3157827.

[36] B. Wang, D. Wang, J. Nie, W. Miao, C. Wang, and X. Wang, "Zero-order electromagnetic vibration suppression of permanent magnet synchronous motor with harmonic currents injection," *IEEE Trans. Magn.*, vol. 61, no. 2, pp. 1–5, Feb. 2025, doi: 10.1109/TMAG.2024.3519574.

[37] T. Windisch, M. Burkhardt, J. Troge, and W.-G. Drossel, "Reducing tonal noise in IPMSM vehicle drives through harmonic injection," *IEEE Trans. Transport. Electrific.*, vol. 10, no. 1, pp. 1156–1166, Mar. 2024, doi: 10.1109/TTE.2023.3283854.

[38] J. F. Gieras, C. Wang, and J. C. Lai, *Noise of Polyphase Electric Motors*. Boca Raton, FL, USA: CRC Press, 2018.

[39] M. Bösing, "Acoustic modeling of electrical drives: Noise and vibration synthesis based on force response superposition," Ph.D. dissertation, RWTH Aachen Univ., Technische Hochschule, 2014.

[40] *Mathworks*. Accessed: Dec. 11, 2024. [Online]. Available: https://it.mathworks.com/help/sps/ref/inverseparktransform.html

[41] L. Kang, J. Xia, H. Su, Z. Li, and S. Liu, "Online control strategy for radial vibration suppression of PMSM by multiharmonic current injection method," *IEEE Trans. Ind. Electron.*, vol. 69, no. 9, pp. 8692–8704, Sep. 2022.

[42] J. Zhang, W. Jiang, Z. Zhang, and Z. Zhang, "Study on electromagnetic force in interior permanent magnet synchronous machine with distributed windings," in *Proc. 43rd Annu. Conf. IEEE Ind. Electron. Soc.*, Oct. 2017, pp. 2190–2195.

[43] W. Zhang, Q. Yu, C. Li, J. Gao, and K. Liu, "Torque ripple suppression method of high saturation permanent magnet synchronous motor based on current injection method," *IET Power Electron.*, vol. 17, no. 14, pp. 2026–2038, Nov. 2024.

[44] C. Jędryczka, D. Danielczyk, and W. Szeląg, "Torque ripple minimization of the permanent magnet synchronous machine by modulation of the phase currents," *Sensors*, vol. 20, no. 8, p. 2406, Apr. 2020.

[45] A. Z. Chavoshi, B. M. Dehkordi, and M. Ekramian, "Reduction of torque oscillations in permanent magnet synchronous machine using optimal current injection based on unbalanced load detection," *IEEE Trans. Ind. Electron.*, vol. 71, no. 12, pp. 15372–15382, Dec. 2024, doi: 10.1109/TIE.2024.3384595.

[46] P. Yi, W. Zheng, and X. Li, "Overview of torque ripple minimization methods for permanent magnet synchronous motors based on harmonic injection," *Chin. J. Electr. Eng.*, vol. 10, no. 2, pp. 16–29, Jun. 2024.

[47] T. Wolnik, V. Styskala, and T. Mlcak, "Study on the selection of the number of magnetic poles and the slot-pole combinations in fractional slot PMSM motor with a high power density," *Energies*, vol. 15, no. 1, p. 215, Dec. 2021.

[48] J.-W. Jung, J.-P. Hong, and Y.-K. Kim, "Characteristic analysis and comparison of IPMSM for HEV according to pole and slot combination," in *Proc. IEEE Vehicle Power Propuls. Conf.*, Sep. 2007, pp. 778–783.

[49] *LMS Test.Lab*. Accessed: May 24, 2024. [Online]. Available: https://plm.sw.siemens.com/en-U.S./simcenter/physical-testing/testlab/

[50] E. Di Lorenzo, S. Manzato, B. Peeters, F. Marulo, and W. Desmet, "Best practices for using order-based modal analysis for industrial applications," in *Proc. 35th IMAC, Conf. Expo. Struct. Dyn.*, vol. 10. Cham, Switzerland: Springer, 2017, pp. 69–84.

[51] M. G. Joksimovic, E. Levi, and S. N. Vukosavic, "Near-complete suppression of harmonic currents in SPMSMs caused by back EMF and dead time," *IEEE Trans. Ind. Electron.*, vol. 70, no. 5, pp. 4472–4484, May 2023, doi: 10.1109/TIE.2022.3189068.

[52] H. Lin, Y. Liao, L. Yan, F. Li, and Y. Feng, "A novel modulation-based current harmonic control strategy for PMSM considering current measurement error and asymmetric impedance," *IEEE Access*, vol. 10, pp. 89346–89357, 2022.

[53] W. Deng, Z. Qian, W. Chen, C. Qian, and Q. Wang, "Orthotropic material parameters identification method of stator core and windings in electric motors," *IEEE Trans. Energy Convers.*, vol. 38, no. 4, pp. 2464–2474, Dec. 2023.

[54] F. Chai, Y. Li, Y. Pei, and Z. Li, "Accurate modelling and modal analysis of stator system in permanent magnet synchronous motor with concentrated winding for vibration prediction," *IET Electr. Power Appl.*, vol. 12, no. 8, pp. 1225–1232, Sep. 2018.

[55] D. Barri, F. Soresini, F. Ballo, F. Lucà, S. Manzoni, M. Gobbi, and G. Mastinu, "NVH performance of permanent magnet synchronous motors with liquid cooling system," *SAE Int. J. Vehicle Dyn., Stability, NVH*, vol. 9, no. 1, pp. 69–84, Jan. 2025, doi: 10.4271/10-09-01-0004.

[56] F. Orban, "Damping of materials and members in structures," *J. Phys., Conf. Ser.*, vol. 268, no. 1, Jan. 2011, Art. no. 012022.

[57] Schaeffler Group, Herzogenaurach, Germany. (2024). *Schaeffler Bearings*. Accessed: Dec. 13, 2024. [Online]. Available: https://www.schaeffler.com
[58] *ABAQUS 2022 Analysis User Manual*, Dassault Systemes Simulia Corp., Simulia, Johnston, RI, USA, 2022.
[59] F. Lin, S. Zuo, W. Deng, and S. Wu, "Noise prediction and sound quality analysis of variable-speed permanent magnet synchronous motor," *IEEE Trans. Energy Convers.*, vol. 32, no. 2, pp. 698–706, Jun. 2017. [Online]. Available: https://api.semanticscholar.org/CorpusID
[60] P. Hou, B. Ge, D. Tao, Y. Wang, and B. Pan, "Coupling analysis of electromagnetic vibration and noise of FeCo-based permanent-magnet synchronous motor," *Energies*, vol. 15, no. 11, 2022, Art. no. 3888, doi: 10.3390/en15113888. [Online]. Available: https://www.mdpi.com/1996-1073/15/11/3888
[61] B. Klarin, K. Knaus, J. Schneider, F. Diwoky, T. Resch, and S. Brandl, "PMSM noise-simulation measurement comparison," SAE Tech. Paper 2018-01-1552, 2018.

FEDERICO SORESINI received the master's degree (Hons.) in mechanical engineering, in 2020. He is currently pursuing the Ph.D. degree in mechanical engineering with Politecnico di Milano. His main research interests include electric motors NVH simulation and testing, electric motors optimal design, and multi-objective optimization.

DARIO BARRI received the master's degree in mechanical engineering, in 2020. He is currently pursuing the Ph.D. degree in mechanical engineering with the Mechanical Department, Politecnico di Milano, Milan, Italy. He is working on optimal design of electric motors, with a focus on noise, vibration and hardness problems. His research interests include multi-objective optimization and structural and electromagnetic simulations.

FEDERICO BALLO received the Ph.D. degree in mechanical engineering from Politecnico di Milano, Italy, in 2015. He is currently a Research Fellow with Politecnico di Milano. His main research interests include multi-objective optimization of complex systems, structural optimization, numerical modeling of mechanical systems, with particular reference to ground vehicles.

MASSIMILIANO GOBBI received the master's degree (Hons.) in mechanical engineering, in 1994, and the Ph.D. degree in applied mechanics, in 1997. In 1998, he was a Visiting Scholar with the University of California at Berkeley, Berkeley, CA, USA. He is currently a Full Professor with Politecnico di Milano, Milan, Italy. He has authored more than 250 articles. He is the author of ten international patents and three books.